# Chapter 3. TDPAC Study of Group-IVB Oxides in Bulk Dimension

## 3.1. Bulk Oxides:

### 3.1.1. Introduction:

In last two decades, $TiO_2$ has emerged as one of the most important materials in basic research and found applications in different technologically important areas. $TiO_2$, either in pure form or in doped form, has uses as photocatalyst, energy converter in solar cells, white pigment in paints, sunscreen material, just to name a few. $ZrO_2$ is mostly used for its structural properties. The strengthening afforded by its martensitic phase transformation has made it the material of choice for high-temperature applications. Other common applications include fuel cell electrodes, thermal barrier coatings, cutlery and jewelry etc. $HfO_2$ is often thought to be a higher temperature substitute for $ZrO_2$. This is mostly due to the similarities in their chemical properties. $HfO_2$ has uses in nuclear applications also due to its high neutron absorption efficiency. More recently it has found application as high-k dielectric materials and has proved to be a promising candidate to replace $SiO_2$ as the gate oxide in transistors, to obtain electronics with smaller feature sizes.

$TiO_2$, among several natural polymorphs, exists in three main crystalline modifications- rutile, anatase and brookite, each of which occurs naturally. Of these, rutile is the most stable form. Other forms are converted into rutile on heating. Each contains 6 coordinate Ti but rutile is the most common form, both in nature and as produced commercially. The rutile structure is based on slightly distorted hcp of oxygen atoms with half the octahedral interstices being occupied by Ti atoms. Anatase and brookite are both based on cubic rather than hexagonal close packing of oxygen atoms, but again the Ti atoms occupy half the octahedral interstices. At room

temperature, $ZrO_2$ (baddeleyite) and isomorphous $HfO_2$ have a monoclinic structure in which the metal is 7-coordinated.

In the present work, two nuclear probes $^{181}Hf/^{181}Ta$ and $^{111}In/^{111}Cd$ have been introduced into the bulk matrix of Ti, Zr and Hf-oxides during the chemical preparation of these oxides so that the probe can occupy a definite lattice site in these oxide matrices. It is expected that Hf, being the same group element with similar ionic radii in +4 state, can replace the metal site even in the the other two oxides, i.e., $TiO_2$ and $ZrO_2$. For the structure of rutile an axially asymmetric EFG at the Ti site is expected. Anatase, on the other hand, for its structural symmetry, is expected to have an axially symmetric EFG. However, a small non zero asymmetry has been observed with a $^{44}Sc$ probe [194]. In the present work, two probes have been used to find out the TDPAC parameters. Furthermore, the chemistry of the probes used in this work with the host matrices is also different. The quadrupole interaction parameters can thus be good tools to understand the probe-host interaction. Another aspect concerning the dependence of the EFG on the mother isotope i.e. the origin of the probe or decay mode through which the probe is formed has been addressed in this present work.

Both $HfO_2$ and $ZrO_2$ have monoclinic structure with almost similar unit cell dimensions. So it is expected that they will have identical TDPAC parameters. The TDPAC parameters for the bulk have also been measured with two probes, viz., $^{181}Hf/^{181}Ta$ and $^{111}In/^{111}Cd$. $In^{3+}$ ion has an ionic radius radius of 0.81Å which matches closely to that of $Ti^{4+}$ (0.68Å), $Hf^{4+}$ (0.81Å) and $Zr^{4+}$ (0.80Å) ions.

### 3.1.2. Sample Preparation:

In case of the $^{181}Hf/^{181}Ta$ probe, it was produced by neutron irradiation in a thermal neutron-flux of ~$5x10^{13}$ $n/cm^2/s$ at Dhruba Reactor, BARC, Mumbai by the reaction $^{180}Hf$ (n,γ) $^{181}Hf$. The

second probe was produced by the α-beam facility at Variable Energy Cyclotron Centre, Kolkata via the reaction $^{nat}$Ag ($\alpha$, $xn$) $^{111}$In at $E_\alpha$ = 30 MeV and I= 500-600 nA. The $^{111}$In activity was separated in carrier-free form by a radiochemical separation method. The irradiated Ag-foil was dissolved in conc. $HNO_3$, diluted with water and then precipitated as AgCl by addition of Conc. HCl dropwise till complete precipitation. The precipitate was isolated by centrifugation and the solution contained the $^{111}$In –activity in carrier free form. Ti-isopropoxide, Zr-oxychloride and Hf-oxychloride were used as the precursor for $TiO_2$, $ZrO_2$ and $HfO_2$ respectively. The probes were introduced in the matrix during their preparations via the coprecipitation method. The probe was added at a very low concentration (<0.01 atom%) so that the crystal structures of the host matrices remain unaffected. The required amount of the precursors was dissolved in dil. HCl and then the probe solution was added to it. The metal-hydroxides were precipitated along with the probe by the addition of ammonia solution. The precipitates were thoroughly washed with water to remove any ammonia. They were then dried and annealed under different conditions to produce the respective oxides. It was observed that $TiO_2$ annealed at 823K/4h remained in the anatase phase and it was converted into rutile phase at 1123K/4h. For $ZrO_2$ and $HfO_2$, the respective samples were annealed at 1273K for 20h.

### 3.1.3. Results and Discussion:

TDPAC spectra for the anatase and rutile $TiO_2$ with $^{181}$Ta probe are shown in Figure 3.1. On the left of the figure are shown the $A_2G_2$ spectra and the corresponding cosine transforms are shown on the right. From the $A_2G_2$ spectra, it is seen that rutile gives a sharper pattern than anatase. However, a well-defined pattern of $A_2G_2$ indicates that the probe atom could occupy a definite lattice site in the present matrices. So, the present method of sample preparation via coprecipitation method is proved to be a very mild chemical method where the probe atom could

occupy definite lattice position during the preparation of the host matrix. Although the TDPAC results for rutile were previously known [195], the same for anatase was measured for the first time. Again the method for sample preparation is also different from the previous works.

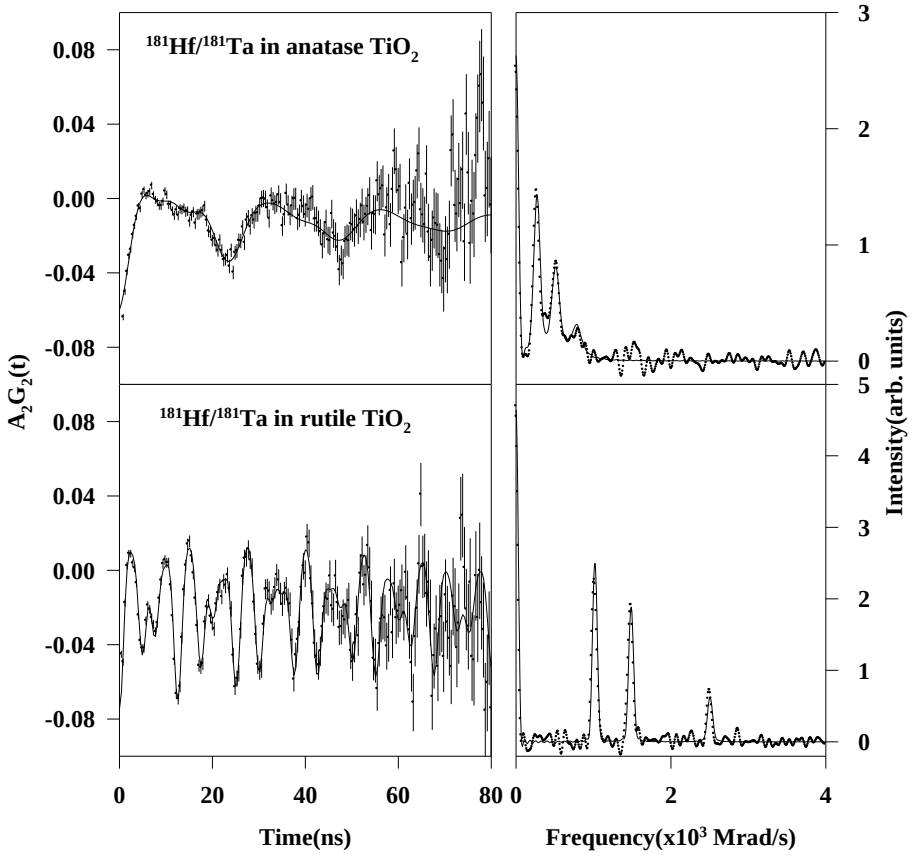


**Figure 3.1:** TDPAC spectra with cosine transform for anatase and rutile with $^{181}$Ta probe.

For both $HfO_2$ and $ZrO_2$, the spectra appear to identical and hence a representative TDPAC spectrum for both $HfO_2$ and $ZrO_2$ is shown in Figure 3.2. The spectrum represents the monoclinic structure around the probe atom. In case of $HfO_2$, the probe becomes the indegeneous probe but in case $ZrO_2$, it is expected that Hf atom could replace the Zr-atom in the $ZrO_2$ matrix. The well-defined $A_2G_2(t)$ pattern confirms that the $^{181}$Hf atom could substitute the Zr-site. Hence

from the TDPAC measurements, it can be concluded that the present probe $^{181}Hf/^{181}Ta$ could occupy the lattice sites in all the three oxides to give well-defined spetra

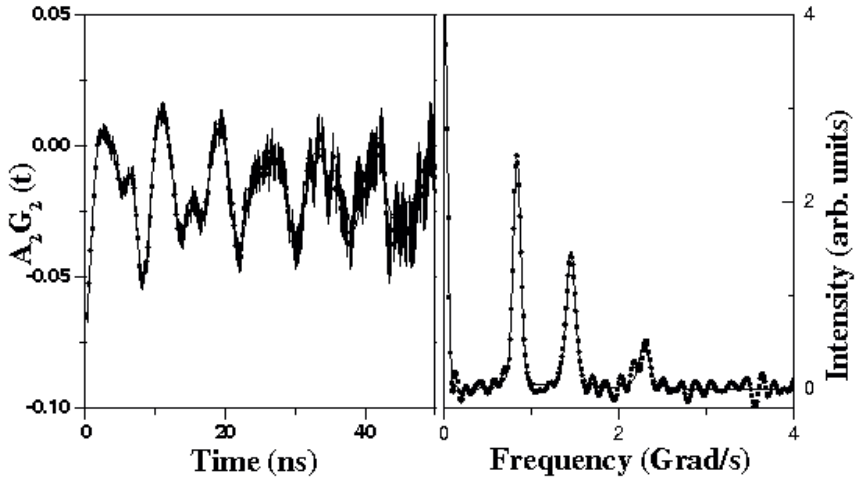


**Figure 3.2:** Representative TDPAC spectra with cosine transform for $HfO_2$ and $ZrO_2$.

The TDPAC parameters for these three oxides for $^{181}Hf/^{181}Ta$ probe are furnished in Table 3.1.

**Table 3.1: TDPAC parameters for $^{181}Hf/^{181}Ta$ probe**

| Samples | $\omega_Q$ (Mrad/s) | $\eta$ | $\delta$ (%) |
|---|---|---|---|
| Anatase $TiO_2$ | 44.01(3) | 0.22(1) | 3.2 (1) |
| Rutile $TiO_2$ | 130.07(9) | 0.56(1) | 1.1 (1) |
| Pure $ZrO_2$ | 124.1 (5) | 0.35 (1) | 3.3 (3) |
| Pure $HfO_2$ | 126.1 (1) | 0.36 (1) | 6.4 (1) |

Any probe other than the indigenous atom Ti is an impurity in the $TiO_2$ chemical bonding of this impurity with the host matrix is different than in the indigenous matrix leading to the difference in the hyperfine parameters for different probes. The crystal symmetry in anatase is 4m2 which implies axial symmetry ($\eta = 0$). However the nonzero $\eta$ (=0.22) for the probe $^{181}Ta$ can be

attributed partly due to the relatively large distribution width of $\omega_Q$. The poor crystallinity due to the low temperature annealing was probably responsible for this observation. The width of the frequency distribution for the anatase phase in this sample also was relatively large and it could not be improved to the extent of rutile. Another reason for the nonzero $\eta$ could be the 0.1% impurity due to the probe nucleus in the $TiO_2$ matrix. The strength of EFG is more in case of rutile than that in case of anatase. This can be explained in terms of the O-positions in the lattice around the probe nucleus. There are two sets of O- atoms around the probe atom: four O- neighbours (with M-O distance, say, d1) and two O- neighbours (with M-O distance, say, d2) in the $MO_6$ octahedra. The calculated values of d1 and d2 in anatase and rutile phases vary depending on the probe and the number of electrons to be added over the indigenous Ti ion. It is found [196] that though d1 increases, there is a decrease in d2 in rutile compared to those in anatase. Using these M-O parameters, $V_{zz}$ in rutile has been found to be larger in rutile for the present probe [197].

The second probe $^{111}In/^{111}Cd$, incarriier free form was introduced into these three oxides via the same coprecipitation method. The TDPAC spectrum for rutile matrix with the $^{111}In/^{111}Cd$ probe is shown in Fig. 3.3.

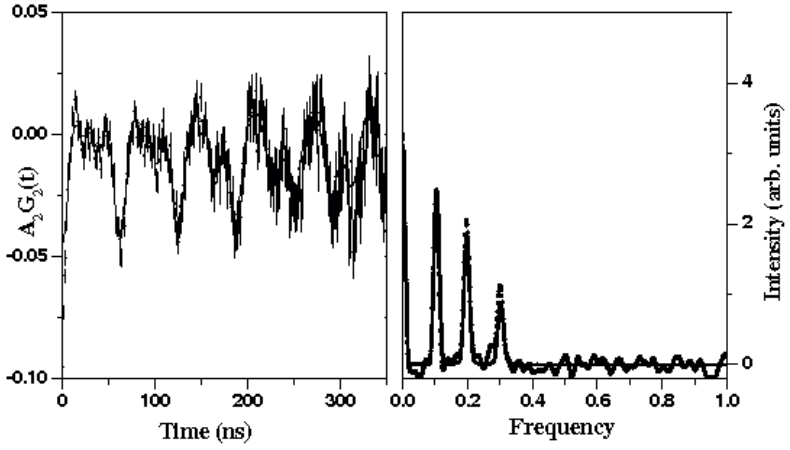


**Figure 3.3:** TDPAC spectra with cosine transform for rutile $TiO_2$ with $^{111}In$ probe.

In case of rutile structure, the probe could occupy the Ti-sites in the crystal to give the well-defined TDPAC spectrum. A representative TDPAC spectrum for $ZrO_2$ and $HfO_2$ with the $^{111}In/^{111}Cd$ probe is shown in Fig. 3.4.

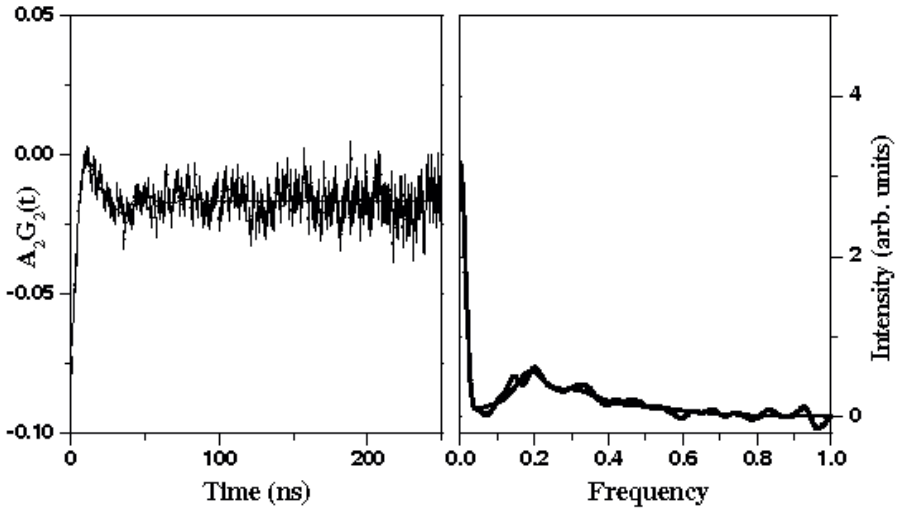


**Figure 3.4:** Representative TDPAC spectrum for $HfO_2$ and $ZrO_2$ with $^{111}In$ probe.

In both $ZrO_2$ and $HfO_2$, $^{111}In$ does not seem to occupy a definite site as there is large damping. The TDPAC parameters for the three oxides with $^{111}In/^{111}Cd$ probe are furnished in Table 3.2.

**Table 3.2: TDPAC parameters for $^{111}In/^{111}Cd$ probe**

| Samples | $\omega_Q$ (Mrad/s) | $\eta$ | $\delta$ (%) |
|---|---|---|---|
| Rutile $TiO_2$ | 16.6 (2) | 0.2 (1) | 1.1 (1) |
| Pure $ZrO_2$ | 25.9 (3) | 0.33 (2) | 23.3 (3) |
| Pure $HfO_2$ | 27.1 (1) | 0.39 (2) | 25.4 (1) |

$^{111}Cd$ probe finds definite site in rutile $TiO_2$ but not in $ZrO_2$ and $HfO_2$. However, in both $ZrO_2$ and $HfO_2$, the results are very close which is expected as these two have same crystal structure. To remove the doubt of sample preparation, $HfO_2$ was prepared in the same condition with $^{181}Hf$ probe. This sample shows clearly definite site occupancy in the TDPAC spectrum. It was thus

confirmed that the monoclinic phase of $HfO_2$ and $ZrO_2$ is attained under the present annealing condition. So either the $In^{3+}$-ion could not occupy the lattice site in these two oxides while it could occupy the lattice site in rutile or the correlation is attenuated by the preceeding decay feeding the cascade. $In^{3+}$ ion has a radius (0.81Å) which is close to those of $Hf^{4+}$ (0.81Å) and $Zr^{4+}$ (0.80Å) ions but different from $Ti^{4+}$ (0.68Å) ion. $In^{3+}$ is thus expected to replace more easily the Hf/Zr ions than Ti ion. Another sample was prepared even at a higher annealing condition (1673K/4h) when the similar spectrum with large damping was obtained. So it might be due to the after effects of EC-decay of $^{111}$In feeding the cascade. The symmetry around the probe atoms is not disturbed while the system could not attain fully crystalline phase. The absence of any time dependant part in the perturbation factor excluded the possibility of oxygen hopping.

### 3.2. Doped Oxides:

#### 3.2.1. Introduction:

It is known that either by reducing the dimension of the material or by doping with suitable metal ion, the material property can be tailor-made to adopt it for a particular application. There has been an extensive study on the effect of transitional metal ion doping and rare earth metal ion doping for enhancing the photocatalytic efficiency of titania. The optical properties of $TiO_2$ can be tuned properly by suitable dopants for its use in different applications. Again, for another important application of the photocatalytic property of $TiO_2$ towards the hydrogen production, it is required to adjust band-gap of $TiO_2$. For this purpose, $TiO_2$ is doped with transition metal ions (Fe, Mn, Ni, Cr etc.) and non-metals (N, S, C, B etc.). Noble metals, including Pt, Au, Pd, Rh, Ni, Cu and Ag, have also been found to be very effective for enhancing the photocatalytic efficiency of $TiO_2$. For iron doped $TiO_2$ [198] has been found to absorb at higher wavelength than the pure one and it thus suits for a photo catalyst at the visible radiation range. The other

two oxides, namely $HfO_2$ and $ZrO_2$ have found their applications in different phase including high-temperature phases. There have been a number of studies on the stabilization of high-temperature phases by doping with suitable elements. The doping with a tetravalent cation (same valence as of $Hf^{4+}$ and $Zr^{4+}$) with a larger ionic radius than that of $Hf^{4+}$ or $Zr^{4+}$ ions leads to an enlargement of the crystal system in order to accommodate the larger ion resulting in the stabilization of the high temperature phases. Again, the doping with a cation having a lower valence than the $Hf^{4+}$ or $Zr^{4+}$ ions introduces oxygen vacancies which play a key role in the stabilization of the high temperature phases. The Mn-dopant stabilizes the cubic phase of hafnia. The variable valences of Mn leading to the different ionic-sizes of Mn and the oxygen vacancies play an important role to stabilize the cubic phase.

The mechanism of the material modification by doping of certain ion is not clearly understood so far. Several possibilities are: (i) the variable valency of Ti, (ii) the edge sharing of $TiO_6$ octahedron, (iii) the unpaired d-electrons of the transition metal ions, (iv) the oxygen vaccancies, (v) metal-metal interaction. In the TDPAC experiment one exploits the perturbation of the angular correlation of the cascade photons emitted by the probe nucleus attached to the matrix under study. The perturbation is caused by the interaction between the nuclear quadrupole moment of the probe nucleus and the EFG around it. This EFG and its asymmetry obtained from the TDPAC experiment describe the electron distribution around the probe atom. This is again decided by the arrangement of the atoms in the lattice and the electron sharing between the probe and surrounding atoms or ions. In general, the probe is not the same indigenous atom of the host lattice. The probe thus acts as an impurity in the lattice. However it is added in very insignificant quantity and thus it does not affect the overall lattice structure. But the hyperfine parameters mentioned are not same compared to the situation where the probe and the host atoms are same.

These parameters give the information about the microscopic aspects of the lattice with atomic scale resolution. If the lattice is doped with some foreign impurity in significant concentration, the lattice structure or the electron distribution around the probe atom would change and it would be reflected in the hyperfine parameters. Therefore the TDPAC results would be of great help in describing the possible mechanism of the aforesaid modification of $TiO_2$ by doping with different dopants. In the present work, rutile matrix has been doped with one transition element Mn and another same group element Zr. The effect of the doping has been investigated with the TDPAC method. The $^{181}Hf/^{181}Ta$ was used as the PAC probe in the present study.

**3.2.2. Sample Preparation:**

The same coprecipitation method was followed for the preparation of the doped sample. For Mn-doped sample, a required amount of $MnCl_2.4H_2O$ salt was added along with the probe solution to prepare the 5 atom% Mn-doped anatase and rutile samples. For Zr-doped rutile sample, the required amount of Zr was added in the form of $ZrOCl_2.8H_2O$. The amount of Zr-atom was adjusted to get the $TiO_2$ samples of 1, 5 and 10 atom% of Zr.

**3.2.3. Results and Discussion:**

The TDPAC spectrum for 5% Mn-doped anatase $TiO_2$ is shown in Fig. 3.5

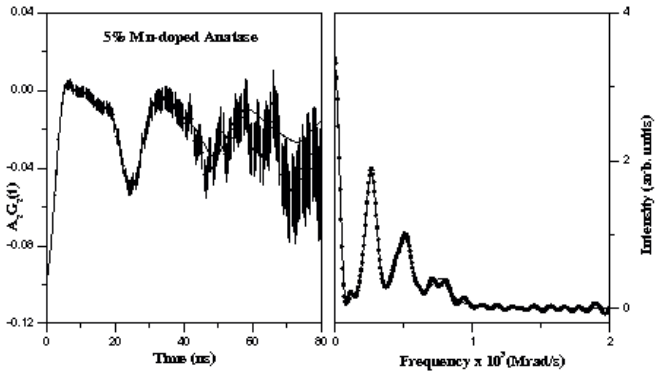


**Figure 3.5:** TDPAC spectrum for 5% Mn-doped anatase $TiO_2$.

and the corresponding spectrum for rutile is shown in Fig. 3.6.

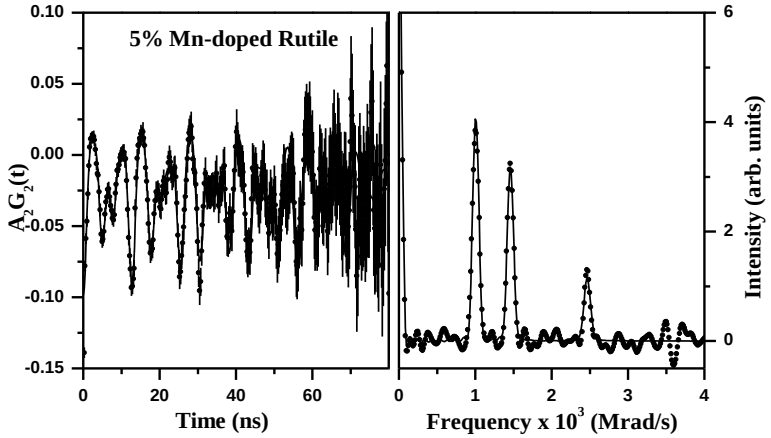


**Figure 3.6:** TDPAC spectrum for 5% Mn-doped rutile $TiO_2$.

The TDPAC parameters for the doped systems match very closely with that for the pure systems. The Mn-ion could occupy definite lattice structure in both anatase and rutile structures. The similar hyperfine parameters indicate that the probe-metal interaction remains same both in pure and doped systems. However, the distribution of frequency in doped systemis higher than that in pure system indicating a higher degree of inhomogeneity in doped matrices.

The TDPAC spectrum for 1% Zr-doped rutile is shown in Fig. 3.7.

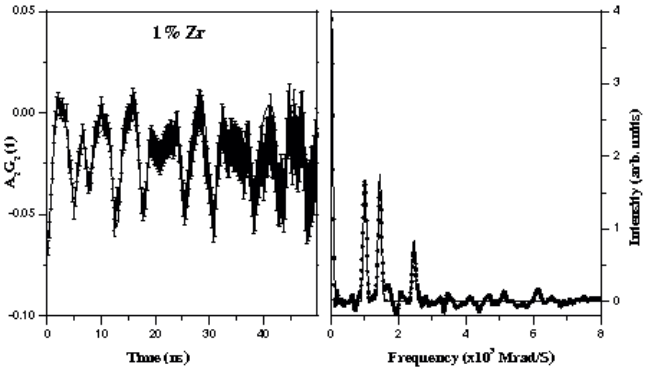


**Figure 3.7:** TDPAC spectrum for 1% Zr-doped rutile $TiO_2$.

The spectrum closely resembles to that for the pure rutile system. The TDPAC spectra for rutile systems doped with 5 and 10 atom% of Zr are shown in Fig. 3.8.

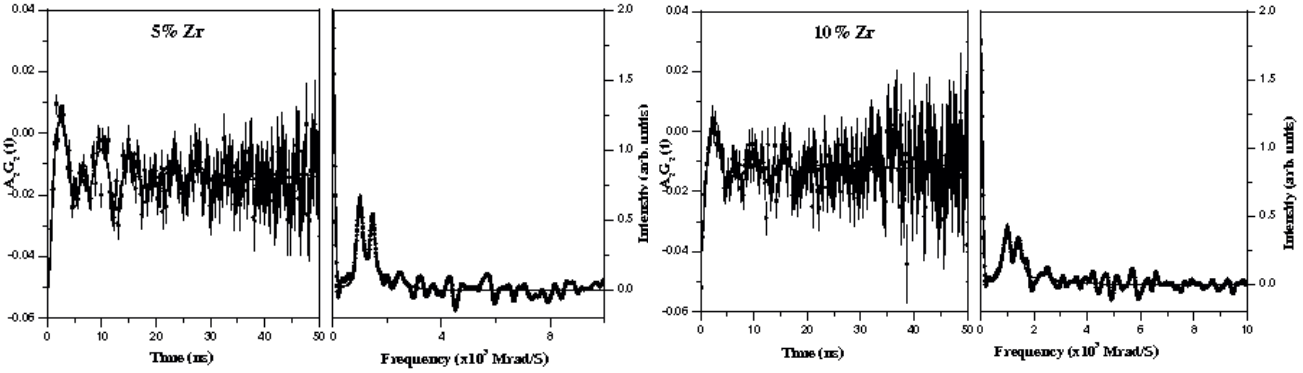


**Figure 3.8:** TDPAC spectra for 5% (left) and 10% (right) Zr -doped rutile $TiO_2$.

The fitted TDPAC parameters are shown in the Table 3.3.

**Table 3.3**: TDPAC parameters for Zr-doped rutile different samples

| Samples | $\omega_Q$ (Grad/S) | η | δ (%) |
|---|---|---|---|
| Pure rutile | 130.07(9) | 0.56(1) | 1.1(1) |
| 1% Zr/rutile | 127.04(4) | 0.55(1) | 1.3(1) |
| 5% Zr/rutile | 126.2(3) | 0.58(1) | 8.3(9) |
| 10% Zr/rutile | 127.44(7) | 0.55(3) | 12.8(5) |

Rutile $TiO_2$ has a tetragonal structure with space group P42/mnm. In this, the Ti atom is surrounded by eight O atoms as the nearest neighbors in an octahedral geometry. In the next layer there are eight Ti atoms in the corner of the tetragon. The important feature of the rutile structure is that the O-O contacts in the $MO_6$ octahedron are not same and possibly the base of the octahedron is not a square. Similarly the M-O bonds may or may not be of same length. They may be apically elongated or compressed. This tetragonal distortion gives rise to the non zero asymmetry of the EFG [197]. Another important feature of the rutile structure is the role played

by the M-M interaction in the tetragonal distortion. In this present work we looked into this aspect by doping with Zr having same chemical nature of the indigenous Ti atom. $Zr^{+4}$ has an ionic radius of 0.8 Å which almost resembles to that of $Ti^{+4}$ (0.7 Å) and hence, $Zr^{+4}$ is expected to replace the $Ti^{+4}$ site in the rutile structure. In the present situation, Zr atoms are statistically distributed and there is maximum one Zr atom in each unit cell of the $TiO_2$ matrix for the 10 atom% sample. In the lower concentration of Zr the chance of one Zr atom in each unit cell is still less. The results in this work indicate that interaction frequency and the asymmetry parameter remain more or less same. But the distribution (δ) of the frequency is increased steadily with Zr concentration. This tells that the M-M interaction between the central atom (here it is the probe $^{181}Ta$) with metal atoms in the next nearest neighbor exists and they are different in case of Zr than when all atoms were Ti. The statistical distribution of the Zr atoms in the unit cell of $TiO_2$ gives rise to the increase in the width of the frequency distribution. One of the important areas of interest in the rutile structure [199] is the cation-cation interaction which has been looked into in this present work [200] by doping Zr atom being the same chemical counterpart of the indigenous atom Ti. The interaction between the probe and the Zr atom are different than that with the host atoms. This is not reflected in the mean values of the interaction frequency and the asymmetry parameter. The width of the frequency distribution has been found to increase steadily with the Zr concentration. So the hyperfine technique TDPAC can be utilized to investigate the role of dopant in the host matrix and its interaction with the host atoms. The effect of varying concentration of dopant can also be looked into by this microscopic tool.

### 3.3. Radiation Damage Study:

#### 3.3.1. Introduction:

The effect of γ-irradiation on the crystal structure of $TiO_2$ has been attempted by following the leaching behavior of $^{181}Hf$ from the $TiO_2$ matrix as well as by the present hyperfine tool TDPAC. Radioactive wastes remain an imposing problem for safe disposal. Considerable efforts have been extended in this direction. The immobilization processes involve the conversion of the wastes to chemically and physically stable forms in order to minimize the leaching of the radioactivity during storage, transport and disposal. The most frequently applied methods for the immobilization are cementation, bituminization or incorporation into polymers. There has recently been an increased interest in the use of mobile units to condition radioactive waste from nuclear power plants [201]. Immobilisation in a chemically durable matrix has been highlighted for the disposal of long-lived waste. $TiO_2$ has great potential as an advanced high-level nuclear waste form as discussed by Adelhelm et al. [202]. Higher actinides have been found to be the major component of high-level nuclear waste. In this work, the leaching behavior of actinides embedded in the $TiO_2$ matrix has been simulated using the lower homologue hafnium which can replace the lattice site of Ti in $TiO_2$ matrix [197]. After incorporating $^{181}Hf$ tracer into $TiO_2$ matrix, the leaching property of the resulting matrix was studied in water, sodium chloride and humic acid solutions. The leaching was measured in each of the case by following the radioactivity of $^{181}Hf$. $TiO_2$ matrix has also been exposed to γ-radiation field. For this, the leaching of Hf from $TiO_2$ matrix has been investigated in different media, like, water, NaCl solution and humic acid solution. The selection of the leaching media stems from the fact that water is the most common medium of contact, NaCl solution simulates the medium of sea-water and humic acid solution represents the soil environment. In all the cases, the leaching has been

monitored by following the radioactivity of $^{181}$Hf tracer. The effect of γ-dose on the crystal structure of $TiO_2$ has been investigated with the hyperfine interaction technique, viz., TDPAC and it has been correlated with the leaching behavior of $TiO_2$.

### 3.3.2. Sample Preparation:

A stock solution of $^{181}$Hf tracer with 0.1572mg/ml hafnium was prepared by dissolving neutron-irradiated $HfCl_4$ in dilute HCl. $TiO_2$ was prepared from Ti-isopropoxide and $^{181}$Hf was incorporated in situ during the preparation of $TiO_2$. $TiO_2$ was prepared from Ti-isopropoxide and $^{181}$Hf was incorporated in situ during the preparation of $TiO_2$. 300µl of stock $^{181}$Hf solution was taken in 10ml of 3(N) HCl and 7ml of Ti-isopropoxide solution was added to it dropwise resulting in the formation of white lump. It was stirred until the lump was dissolved and a clear solution was obtained. To this solution, ammonia solution was added dropwise to obtain a white precipitate doped with $^{181}$Hf. The white precipitate was filtered off and washed with water several times. Then, the precipitate was dried and crushed to have $TiO_2$ matrix doped with $^{181}$Hf . The dry precipitate was powdered and sieved through two meshes of sizes 150 and 200 to obtain the particles of mesh-size 150-200. It was then divided in two equal portions. One half was annealed at 823K for 4h to get anatase $TiO_2$ and the other half was annealed at 1123K for 4h to get rutile $TiO_2$, both labeled with $^{181}$Hf tracer. Another set of anatase and rutile samples was prepared following the aforesaid method and then γ-irradiated for 7 days at a dose-rate of 5.3 KGy/h in a $^{60}$Co irradiator at UGC-DAE-CSR, Kolkata. Each sample got an average specific activity of 11,000 Bq/gm with respect to $^{181}$Hf tracer.

### 3.3.3. Leaching Study:

At first, the specific activity of both the anatase and rutile $TiO_2$ doped with $^{181}$Hf was measured by taking a weighed amount of $TiO_2$ and counting on a well-type NaI(Tl) detector. Then, a

measured amount of both anatase and rutile forms of Hf-doped $TiO_2$ sample before γ-irradiation was taken in two separate 100 mL conical flasks. 20 mL of water was added to each of the mixtures and the mixtures were stirred overnight. Each mixture was filtered through Whatmann-42 filter paper and activity of 2 mL of each of the filtrates was measured. Same procedure was followed for 1% aq. sodium chloride solution and 1% aq. humic acid solution. The $TiO_2$ samples after γ-irradiation were taken in two separate conical flasks and leaching was followed as mentioned above. The leaching percentage was calculated from the activity of the leached solution and the initial activity of the starting material.Results are shown in Table 3.4.

**Table 3.4:** Result of leaching of $^{181}Hf$ from different $TiO_2$ samples.

| **Samples** | **Leaching solutions** | **% Leaching** | |
|---|---|---|---|
| | | Anatase | Rutile |
| Pristine | pH4 Solution | 0.43 | 0.38 |
| | 1% aq. NaCl | 0.47 | 0.44 |
| | 1% aq. Humic acid | 0.54 | 0.48 |
| After γ-irradiation | pH4 Solution | 0.35 | 0.32 |
| | 1% aq. NaCl | 0.41 | 0.40 |
| | 1% aq. Humic acid | 0.52 | 0.42 |

### 3.3.4. Results and Discussion:

The percentage leaching has been obtained from the mean values of the radioactivity. These numbers fall within the statistical uncertainty of the counts. This indicates a negligible leaching

for both the anatase and rutile samples. TDPAC spectrum along with its Fourier transform for a typical rutile sample after γ-irradiation is shown in Fig. 3.9.

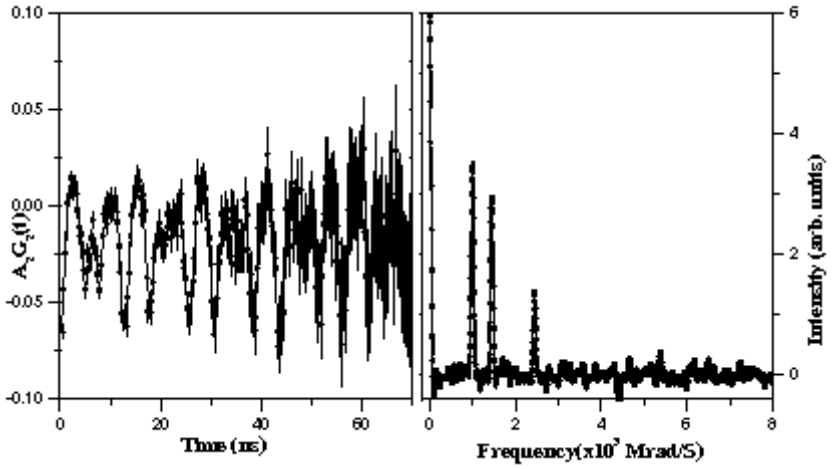


**Figure 3.9:** TDPAC spectrum with cosine transform for γ-irradiated rutile $TiO_2$.

TDPAC parameters for both anatase and rutile $TiO_2$ are shown in Table 3.5.

**Table 3.5:** Hyperfine parameters for rutile $TiO_2$ before and after γ-irradiation.

| Samples | $V_{zz}$ X $10^{17}$ (V/cm$^2$) | | η | | δ | | Comment |
|---|---|---|---|---|---|---|---|
| | Rutile | Anatase | Rutile | Anatase | Rutile | Anatase | |
| Pristine | 13.65 (10) | 4.62 (1) | 0.56 (1) | 0.22 (1) | 0.001 (1) | 0.057 (2) | Ref. 197 |
| After γ-irradiation | 13.41 (02) | 4.64 (2) | 0.57 (1) | 0.23 (1) | 0.001 (1) | 0.058 (2) | This work |

The percentage leaching has been obtained from the mean values of the radioactivity. These numbers fall within the statistical uncertainty of the counts. This indicates a negligible leaching for both the anatase and rutile samples. It is known that rutile form is thermodynamically more stable than anatase form. Rutile is obtained by heating anatase phase at higher temperature (≥1123K) and this is an irreversible process. Both the anatase and rutile forms possess tetragonal

structure with rutile form having shorter and hence stronger metal–oxygen bond. Again, as Ti and Hf fall in the same group, Hf is expected to replace Ti from some of the lattice sites in the $TiO_2$ crystal. So, Hf–O bond is stronger in rutile form than that in anatase and, hence, Hf is expected to be trapped more efficiently in rutile cage than in anatase cage. However, the present study indicates an almost similar extent of leaching of Hf from the anatase and rutile matrices. This might be due to the fact that the bond energy required for entrapping the Hf-ion in $TiO_2$ is sufficient in both anatase and rutile matrices to ensure negligible leaching of Hf-radioactivity. TDPAC parameters shown in Table 3.5 for pure anatase and rutile at $^{181}$Hf site remain unaltered even after γ-irradiation indicating the fact that the Hf–O bond in the matrix is not disturbed by this irradiation. This indicates that the $TiO_2$ matrix has so stable crystal structure that it is not disturbed by a long γ-irradiation and Hf is strongly adhered in the $TiO_2$ matrix. The present leaching study [203] indicates the strong adherence of Hf-ions in the $TiO_2$ matrix in its polymorph, anatase or rutile. Radiation dose has minimal effect on the crystal strucrure of $TiO_2$ and hence on its leaching property. Nuclear probe measurement also corroborates the above observation as the structural change in the $TiO_2$ matrix was insignificant after the irradiation with the γ-dose. The defects, if any, produced by the irradiation was so dilue that it could not interact with the probe. The microstructural aspects of the system are also not disturbed.

## 3.4. Study of $HfO_2$ Fibre:

### 3.4.1. Introduction:

A suitable refractory material which can be heated to elevated temperatures is an essential requirement for an efficient production of the radioactive ion beams (RIB) using the isotope separation on-line (ISOL) technique [204]. At a high temperature, there is a fast release of the product species from the target but at the same time there should not be sufficient vaporization or

sublimation of the target material itself. Among various refractory materials viz. $HfO_2$, $Y_2O_3$, $CeO_2$, $Al_2O_3$ etc. satisfying the physical, chemical, metallurgical and thermodynamical properties, hafnium oxide ($HfO_2$) has been considered as a potential RIB target material [204]. The temperature, at which the vapor pressure of the target material reaches $10^{-4}$ torr, is the highest (2773K) for $HfO_2$. Moreover, Hafnium being the highest Z element among the metal ions of the above mentioned materials, the stopping range of the recoil products is the least in $HfO_2$ and thus the reaction products cannot penetrate the surface and would be released faster increasing the efficiency of the RIB intensity. Fibrous targets of $HfO_2$ have been used successfully for the production of the $^{17}F$ radioactive beam [205]. It has been observed that the $HfO_2$ targets can be operated at a higher temperatures (2373-2573K) compared to the others leading to a more efficient release of the required radioactive isotopes [206]. The properties of the targets using $HfO_2$ in various forms are studied for the RIB facility which is being developed at Variable Energy Cyclotron Centre (VECC), Kolkata incorporating the traditional ISOL technique [207]. According to the simulation studies, it is found that the temperature at the $Al_2O_3$ target would be 1000-2000K depending on the energy deposited by the proton or alpha beam used for the irradiation. It is expected that the $HfO_2$ fibrous targets for the RIB production would be heated to such high temperatures under similar irradiation conditions. In addition, $HfO_2$ has several other applications due to its high mechanical hardness, significant thermal stability and high refractive index. $HfO_2$ having a high dielectric constant can be considered as a gate dielectric in the form of thin film [208]. A recent study [209] describes the annealing behavior of the $HfO_2$ thin film. Since $HfO_2$ undergoes a polymorphic structural transition [210] with the temperature from monoclinic (RT-1443K) to tetragonal (1443-2643K) to cubic (>2645K), it is imperative to study the structural transformation of fibrous $HfO_2$ in this temperature range. In

this present work, the fibrous $HfO_2$ doped with $^{181}Hf/^{181}Ta$ probe was studied using the TDPAC technique where $^{181}Ta$ occupying the Hf sites acted as a TDPAC probe. $HfO_2$ fibrous samples were annealed at different temperatures in 1000-2000K range and the structural aspects were investigated in the samples annealed at such high temperatures using TDPAC technique.

In order to understand the TDPAC results obtained from the $^{181}Ta$ doped $HfO_2$ fibrous sample and also the annealing effects on these samples, we performed the first principle electronic structure calculations based on density functional theory (DFT) [211] using WIEN2K code [212]. We first studied the electronic structures of the bulk $HfO_2$ as we expect that understanding the electronic distribution around the probe $^{181}Ta$ and sources contributing to the electric field gradient (EFG) at the probe site in a bulk sample would lead to a better understanding of the changes that would occur when a fiber or the thin film of $HfO_2$ is prepared and annealed thereafter.

**3.4.2. Experiments and Measurements:**

The $HfO_2$ fiber (make: Zicar Zirconia Inc. USA; purity: 99 wt%) of diameter 6-7μm and density 1.21 $g/cm^3$ was used in the present experiment. $^{181}Hf$ tracer was produced by $^{180}Hf$ (n, γ)$^{181}Hf$ irradiating $HfO_2$ fiber in a thermal neutron flux of $1.0x10^{13}$ neutrons per $cm^2$ per second in DHRUVA reactor at Bhabha Atomic Research Centre, Mumbai, India. A part of the irradiated sample was annealed at 1173K for 6h and other part at 1673K for 6h. Then both the samples were counted for TDPAC at room temperature. The inactive counterparts of the sample, annealed under identical conditions, were used for the XRD and SEM measurements. Bulk $HfO_2$ was prepared by precipitating hafnium hydroxide $Hf(OH)_4$ from $HfCl_4$ solution by adding ammonia solution in presence of $^{181}Hf$ tracer. This precipitate was centrifuged, dried and heated at 1173K for 6 h. This sample was then counted on the TDPAC setup.

### 3.4.3. Results and Discussion:

XRD spectra showed in Fig. 3.10 indicate the lines to correspond to the typical monoclinic $HfO_2$. However, a small increase in the width of the XRD peaks is observed with annealing temperature. This can be qualitatively explained as a partial loss of crystallinity in the $HfO_2$ fiber. A similar trend has also been observed in the TDPAC parameters as mentioned below.

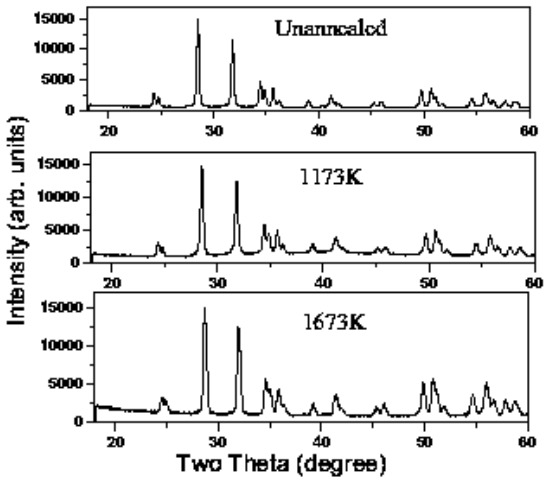


**Figure 3.10:** XRD spectra of the $HfO_2$ fiber annealed at different temperatures.

SEM picture shown in Fig. 3.11 indicates that the fiber, annealed up to 1673K, does not undergo any significant change in its dimension of 6-7μm.

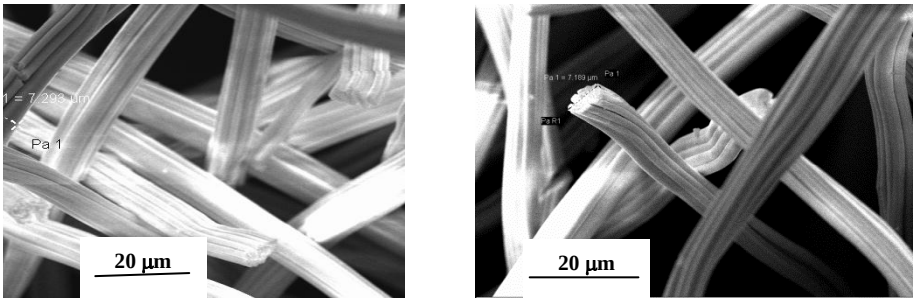


**(a)** **(b)**

**Figure 3.11:** SEM picture of $HfO_2$ fiber annealed at (a) 1173K and (b) 1673K.

TDPAC spectra shown in Fig. 3.12 indicate no change in the electronic structure around the probe atom for all the three samples. However, a small increase in the frequency distribution as shown in Table 3.6 may be attributed to a minor structural change with temperature.

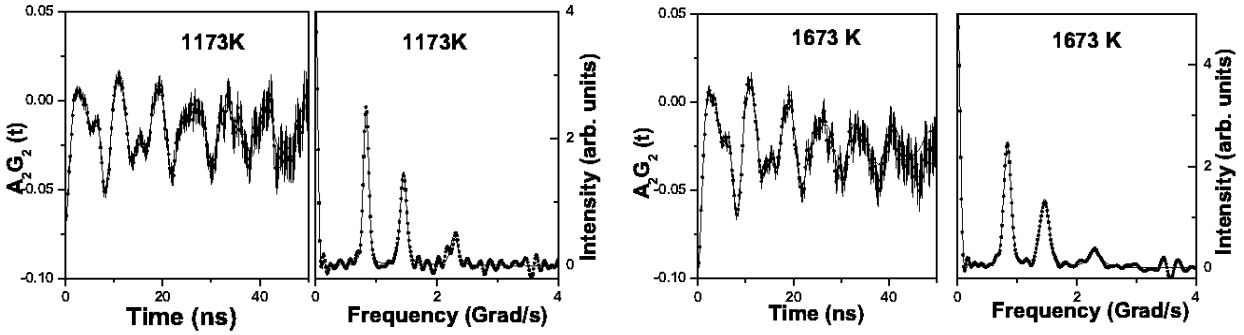


**Figure 3.12:** TDPAC spectra for the $HfO_2$ fiber annealed at different temperatures.

**Table 3.6**: Results for the TDPAC measurements of $HfO_2$ fiber

| $HfO_2$ fiber | $V_{ZZ}$ x $10^{21}$ ($V/m^2$) | η | δ (%) |
|---|---|---|---|
| **Unannealed** | 13.08 (1) | 0.35(1) | 2.6(2) |
| **Annealed at 1173K** | 13.01 (1) | 0.36(1) | 3.0(1) |
| **Annealed at 1673K** | 13.08 (1) | 0.35(1) | 3.2(2) |
| **Bulk $HfO_2$** | 13.04 (2) | 0.34 (1) | 2.4 (2) |

### 3.4.4. Wien2K Calculation:

The Linearized Augmented PlaneWave (LAPW) method has proven to be one of the most accurate methods for the computation of the electronic structure of solids within density functional theory. A full-potential LAPW-code for crystalline solids has been developed over a period of more than twenty years. A first copyrighted version was called **WIEN** and it was published by P. Blaha et al. [213]. A new version WIEN2k is based on an alternative basis set. This allows a significant improvement, especially in terms of speed, universality, user-friendliness and new features.

Ab-initio study of the Ta-doped $HfO_2$ bulk samples has recently been done [214] where the effect on EFG parameters around the probe atom due to the charge state considerations has been observed but it has not been elucidated. In the present work, the electronic structure calculations were performed based on the density functional theory (DFT) and the augmented plane wave plus local orbital (APW+LO) method as embodied in the WIEN2K code was used in order to understand the effect of charge state on the EFG parameters. The exchange and correlation effects were included in our calculation using Generalized Gradient Approximation (GGA) [215]. The basic input requirement for these electronic structure calculations of a crystal are the cell settings and lattice parameters. These required structure parameters used in our calculations are the same as mentioned earlier. The crystal structure of $HfO_2$ is monoclinic where there are four $HfO_2$ molecules in each unit cell and each Hf metal ion is surrounded by the seven oxygen atoms. Since the doping of $HfO_2$ samples with $^{181}$Ta probes for the TDPAC studies were produced by irradiating the $HfO_2$ samples with thermal neutrons, the recoil of the probe nucleus is negligible. However, the recoil due to the prompt gamma emission can not be neglected. Though there is an evidence of recoil induced damage [209], it is expected that these will be removed when the sample is annealed at high temperatures in the present experiment. As we know that the electric field gradient which determines the hyperfine parameters being extremely sensitive to the electronic environment around the probe site, the charge state of the probe atom is of a prime consideration. In order to decide whether Ta would remain in 5+ state at the probe site as it would exist in a pure tantalum compound or there would be a change in the charge state of the probe Ta atom, two independent calculations were performed. In one case it was assumed that there is no change in the charge state of the dopant Ta atom as it replaced Hf atom and called it as neutral state calculations. It was found partially filled impurity levels having Ta "*d"* and

oxygen "*p*" character. In the second case referred to as the charge state calculation, it was assumed that tantalum would act as a donor impurity. So, one valance electron was removed from the unit cell, neutralized the charge by adding one electron to the homogeneous negative background and thereafter performed the self consistent calculations. It is interesting to note that the variation in EFG parameter around the probe atom Ta considering the neutral and charge state configurations is in agreement with the earlier work [213]. There is a speculation that Ta exists in two different charge states in Ta-doped monoclinic $HfO_2$ and considerable amount of the magnetic moment can be induced depending on impurity charge state [216]. The $V_{zz}$ component of EFG for different *l*-projected states was determined and the contribution to EFG at Ta site from the electrons having different *l*-values was studied. In the calculation, one of the Hf atoms of the host $HfO_2$ was replaced by a probe Ta atom in the unit cell i.e. a Ta concentration of 25% ($Hf_{0.75}Ta_{0.25}O_2$) was considered as shown in Fig. 3.13.

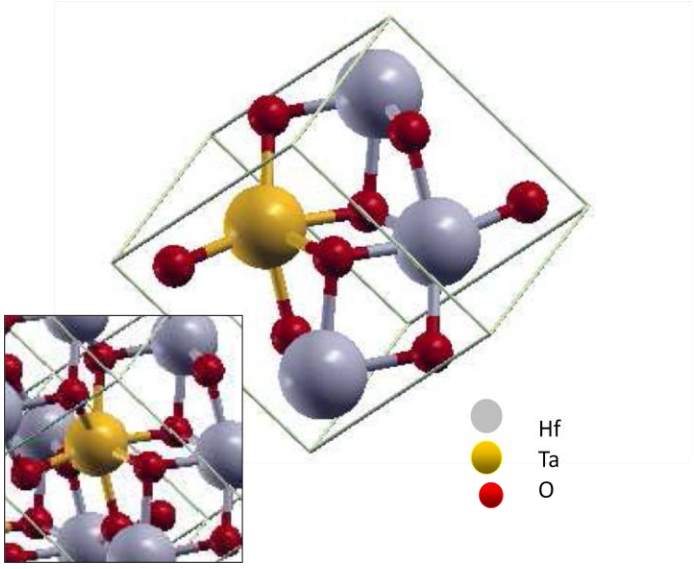


**Figure 3.13:** $HfO_2$ crystal doped with Ta

The probe atom Ta also exhibits a sevenfold-coordination with the Oxygen atoms as shown in the left panel of figure4. When a group-VB tantalum atom replaces a group-IVB hafnium atom,

charge state consideration is of a fundamental significance. In $HfO_2$ crystal, hafnium is expected to exist in 4+ charge state whereas Ta, the substituted probe atom normally exists in 5+ charge state. Electronic structure calculations based on DFT for Ta atom replacing an Hf-atom in $HfO_2$ shows that the EFG at the Ta site considering Ta having a charge q=+1 has a reasonable agreement with that of the experimentally measured value. In Table 3.7, it is seen that the EFG value at the probe Ta site is comparatively very large when the neutral state calculations were performed and *l*-state projections indicate that the EFG at the probe Ta site has unusually large contribution from the outer *d*-electrons. On the other hand, when the charged state of Ta was considered, essentially one outer d-electron was delocalized and as a result the d-electron contribution to total EFG at the probe Ta site reduced drastically and it was found that the maximum contribution to EFG was from inner p-electrons.

**Table 3.7:** Comparison between neutral and charged state calculations for $^{181}$Ta doped $HfO_2$ bulk samples

| **$HfO_2$ sample** | **$V_{zz}$(x$10^{21}$ V/m$^2$)** | **$\eta$** | **Calculated EFG components (*l* projections)** | | |
|---|---|---|---|---|---|
| Experimental | 13.06 | 0.34 | p | D | s-d |
| Neutral | 18.78 | 0.18 | 12.07 | 7.10 | 0.21 |
| Charged | 14.62 | 0.44 | 14.37 | 1.27 | 0.23 |

In order to confirm the charge state of the Ta in $HfO_2$, the densities of states (DOS) vs energy for the Ta doped $HfO_2$ obtained from the electronic structure calculations using WIEN2K code considering the charge state of Ta and the neutral state of Ta has been plotted in Fig. 3.14.

Comparing the total DOS (lowest panel) and the f-state projection of impurity Ta (middle panel), a dramatic change in the density of states for the f-electrons of Ta atom was observed but with no significant difference in the density of states of d-electrons (top panel).

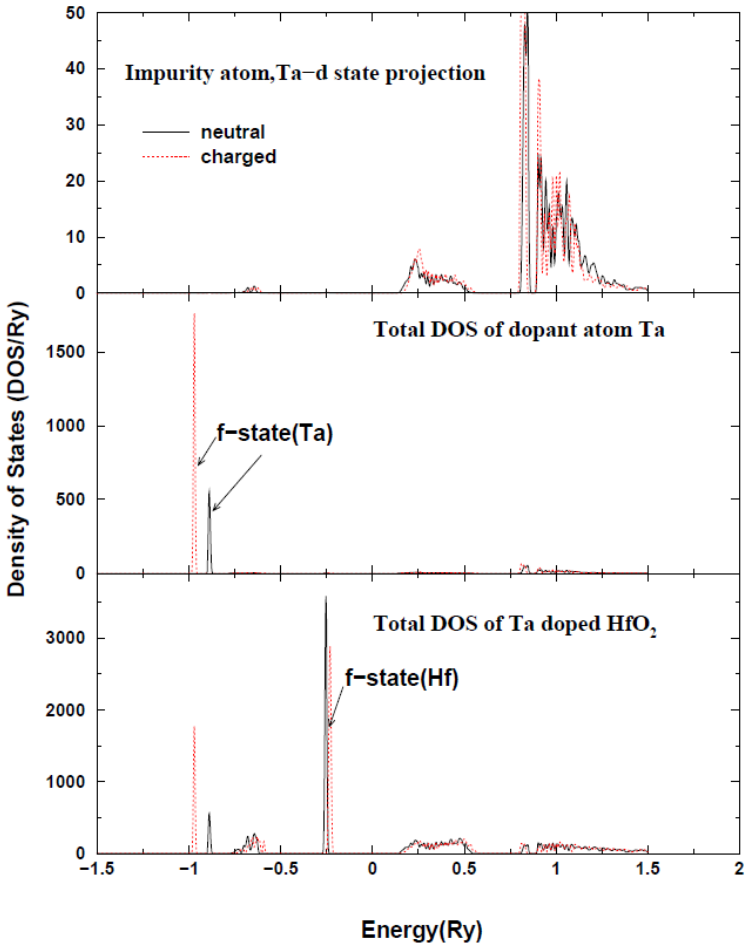


**Figure 3.14**: Lowest panel: Plot of Total Density of states (DOS) vs energy for Ta doped $HfO_2$. Middle panel: Plot of Atom (Ta) projected DOS vs energy, Upper panel: Plot of projected DOS vs energy of probe Ta in $HfO_2$.

The shift in the energy state of the f-electrons indicates that these electrons are more bound when charged state is considered. As the f-electrons screen the outer d-electrons, a reduction in the contribution of the d-electrons was observed and the contribution of the inner p-electrons to EFG is enhanced due to the shift in f-level electrons. Thus we conclude from the experimental

measurement of EFG and electronic structure calculations that the probe Ta in the $HfO_2$ matrix would remain in a charged state configuration and the inner p-electrons would contribute the most to the EFG at the probe Ta site.

The density of states calculated for Ta doped $HfO_2$ samples were compared with that of pure undoped $HfO_2$. In Fig. 3.15, it was found that the density of states at the neighboring Hf site Hf1, Hf2, Hf3 calculated considering the neutral state of Ta, essentially remain unaffected when the $HfO_2$ sample is doped with Ta (upper panel) compared to pure $HfO_2$ as shown in the lowest panel.

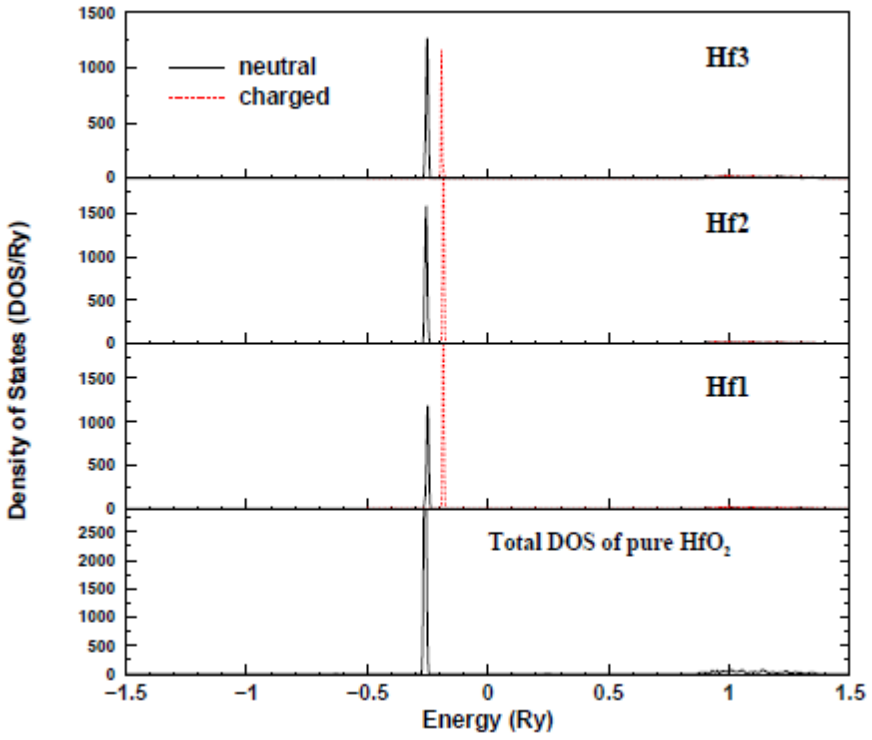


**Figure 3.15:** Lowest panel: Plot of Density of states vs energy for pure $HfO_2$. Upper panel: Plot of atom projected density of states vs energy of nearest neighbor of probe Ta.

This is due to the seven-fold coordination of oxygen atoms surrounding the probe and thus EFG measurements give only localized information around the probe Ta. As a result, 6-7 μm diameter fiber of $HfO_2$, behaves as a bulk sample and no change in EFG parameter is observed during

experimental measurement of doped fibers. As some structural stress developed when Ta replaced Hf in $HfO_2$, the system was allowed to undergo structural relaxations and calculations were performed at several stages till the stress was minimized.

**Table 3.8:** Change in EFG parameters after relaxation of atomic position.

| **Configuration** | **Total Energy(Ryd)** | **$V_{zz}$ (x $10^{21}$ V/$m^2$)** | **$\eta$** |
|---|---|---|---|
| $HfO_2$-1 | -123045.70388 | 14.843 | 0.44 |
| $HfO_2$-2 | -123045.71232 | 14.977 | 0.42 |
| $HfO_2$-3 | -123045.71386 | 14.986 | 0.41 |
| $HfO_2$-4 | -123045.71428 | 14.987 | 0.42 |
| $HfO_2$-5 | -123045.71433 | 14.989 | 0.42 |

In Table 3.8, a little variation in total energy of $HfO_2$ doped with Ta indicates that the sample has stable configuration even though atomic positions of the neighboring atoms of Ta probe are slightly changed. The existence of the several stable configurations with slightly varying EFG explains the broad distribution in delta when the experimental measurements at room temperature were performed for the sample annealed at 1173K and 1673K.

So the results from XRD, SEM and TDPAC study indicate little change in the structure of the $HfO_2$ fiber annealed upto 1673K. But no phase transition could be observed under the present experimental condition. Thus the $HfO_2$ fiber can well be used as the target material for RIB production. $HfO_2$ fiber of dimension 6-7 μm has essentially the same TDPAC patterns as those of the bulk $HfO_2$. This indicates no difference between the structures of the bulk and the fiber $HfO_2$. However, there is a signature of slight loss of crystallinity in $HfO_2$ annealed at 1173K and 1673K as indicated by the small increase in quadrupole frequency distributions with annealing temperature. DFT calculation of the $HfO_2$ system indicates that the $^{181}$Ta probe is in the charged

state in the lattice position and the contribution of the EFG is mainly due to the p-electrons. Density of states indicates that the doping with Ta does not affect the neighboring Hf atoms of the host. As a result, EFG parameters of the fiber having 6-7 μm diameter doped with Ta are expected to remain unaltered compared to those of bulk $HfO_2$.

**3.5. Conclusion:**

The present TDPAC study in bulk dimension delivers the versatility and sensitivity of the present hyperfine technique TDPAC. A general trend of higher $V_{zz}$ in the rutile phase than in the anatase phase has been observed in this work. This is true for other probes as well and was explained in terms of the O-positions around the probe nucleus. A similar $V_{zz}$ value for $HfO_2$ and $ZrO_2$ systems has also been explained in terms of their similar crystal structure. In general, it has been demonstrated that the TDPAC parameters for a crystal system have a direct correlation with the lattice parameters of that crystal system. The TDPAC parameters for the pure group-IVB oxides in bulk dimension measured with the new coincidence setup involving the latest $LaBr_3$(Ce) detectors would be a guideline for the study of these oxides in other dimensions as well as in doped forms. The method has been applied in the doped anatase and rutile systems for the first time. The minute effect on the crystal structure of the system with increasing dopant concentration has been demonstrated with the TDPAC technique. These data would also offer a guideline to study the doped nano $TiO_2$ having versatile applications. The stability of the $TiO_2$ structure against γ-irradiation as studied by TDPAC in the present work would inspire a further study of this system for the immobilization of long-lived nuclear waste. The present work on the HfO2 fiber concludes that this oxide does not undergo either any significant structural change or any phase transition and hence it can be used as the target material for RIB production upto an annealing temperature of 1673K.